

IMAGE RECONSTRUCTION OF UPPER LIMB BONE FRACTURES USING
ELECTRICAL IMPEDANCE TOMOGRAPHY ON PYTHON FRAMEWORK

ABDUL SALAM A HARIS

A thesis submitted in fulfilment of the
requirements for the award of the degree of
Master of Philosophy

School of Biomedical Engineering and Health Sciences
Faculty of Engineering
Universiti Teknologi Malaysia

APRIL 2022

DEDICATION

In the name of Allah, the Most Gracious and the Most Merciful.

All praises to Allah and His blessing for the completion of this thesis. I thank God for all the opportunities, trials and strengths that have been showered on me to finish writing the thesis. I experienced so much during this process, not only from the academic aspect but also from the aspect of personality. My humblest gratitude to the Holy Prophet Muhammad (Peace be upon him) whose way of life has been continuous guidance for me.

This thesis is dedicated to my supervisor Dr. Mohd Najeb bin Jamaludin, my co-supervisor Dr. Muhammad Amir bin As'ari for continuous support and encouragement. Also, my family and all my colleagues that help me to overcome hurdle in completion of this thesis.

ACKNOWLEDGEMENT

In preparing this thesis, I was in contact with many people, researchers, academicians, and practitioners. They have contributed towards my understanding and thoughts. I wish to express my sincere appreciation to my main thesis supervisor, Dr. Mohd Najeb bin Jamaludin, for encouragement, guidance, advice, and motivation. Without their continued support and interest, this thesis would not have been the same as presented here.

I am grateful to all my family members especially my parent A Haris bin Sulaiman and Harisun binti Ahmad for the sacrifices and efforts I was unable to reciprocate, the constant commitment and guidance, and providing me with lessons and knowledge that helped me in facing whatever life challenges lay ahead.

My fellow postgraduate students should also be recognised for their support. I would like to extend my sincere appreciation to all my colleagues and others who have aided at various occasions. Their views and tips are useful indeed. Unfortunately, it is not possible to list all of them in this limited space. May God shower the above mentioned personalities with success and honour in their life.

ABSTRACT

Minor bone fractures could occur due to traumatic incidents such as injuries, vehicle accidents, and falls. The commonly used devices to diagnose for bone fracture are X-ray, Computerized Tomography (CT)-Scan, Positron Emission Tomography (PET)-Scan, and Magnetic Resonance Imaging (MRI). For a series of post diagnosis of bone fracture, it can be health threatening to expose the patient to ionization radiation repeatedly. This research proposes to utilize Electrical Impedance Tomography (EIT) as an invasive modality to monitor the recovery of bone fracture. The aim is to develop EIT circuit to measure the electrical impedance on the phantom model of the upper limb with fractured bones using saline solution and 3D printed bones, the phantom model is reconstructed in 2D images on each cross-section layer using pyEIT and analyze the performance of the reconstructed model of fractured bone. This initiative begins with the development of the EIT circuit system, which consist of sinusoidal waveform generator 100 kHz to 10 MHz frequency range, 32-channel multiplexer unit, instrumentation amplifier with slew rate 35 V/ μ s, bandpass filter range of frequency from 10 kHz to 4 MHz, Root Mean Square (RMS) to Direct Current (DC) converter, 24-bit analog-to-digital converter, flexible Printed Circuit Board (PCB) 32 electrodes per layer, power supply and microcontroller. The EIT circuit is used to acquire voltage measurement using neighboring and opposite data collection techniques from the phantom tank which consist of saline solution (0.9% NaCl) and was tested on 3D printed Acrylonitrile Butadiene Styrene (ABS) bone and lamb bone. The EIT image of the phantom was reconstructed using pyEIT in three-layers slices on 3D plane. Then, the images were analyzed its performance using root mean square error (RMSE) and correlation coefficient. The RMSE value of the reconstructed images at the frequency of 400 kHz was 0.2785 ± 0.01 . From the correlation coefficient between the ABS bone and lamb bone, there are significant similarity in terms of impedance between both materials with Pearson correlation with minimum values of 0.636. It would be beneficial to use the ABS material to simulate the different shape of bone fracture to be reconstructed in EIT system. The fractures are observable on several images. In addition, the depth of the bone is can also be distinguished.

ABSTRAK

Keretakan tulang kecil boleh berlaku disebabkan oleh insiden traumatik seperti kecederaan, kemalangan kenderaan dan terjatuh. Peranti yang biasa digunakan untuk mendiagnosis patah tulang ialah *X-ray*, Tomografi Berkomputer (*CT*)-*Scan*, Tomografi Pelepasan Positron (*PET*)-*Scan*, dan Pengimejan Resonans Magnetik (*MRI*). Untuk satu siri diagnosis pasca patah tulang, boleh membahayakan nyawa untuk mendedahkan pesakit dengan sinaran pengionan berulang kali. Pada penyelidikan ini mencadangkan untuk menggunakan Tomografi Impedansi Elektrik (*EIT*) sebagai modaliti invasif untuk memantau pemulihan patah tulang. Matlamatnya adalah untuk membangunkan litar *EIT* untuk mengukur impedansi elektrik pada model buatan anggota tangan dengan tulang patah menggunakan larutan garam dan tulang cetakan 3D, model buatan telah dibina semula dalam imej 2D pada setiap lapisan keratan rentas menggunakan *pyEIT* dan menganalisis prestasi model tulang patah yang dibina semula. Inisiatif ini bermula dengan pembangunan sistem litar *EIT*, yang terdiri daripada penjana bentuk gelombang sinusoidal 100 *kHz* hingga 10 *MHz* julat frekuensi, unit pemultipleks 32 saluran, penguat instrumentasi dengan kadar *slew* 35 $V/\mu s$, julat penapis laluan jalur frekuensi dari 10 *kHz* kepada 4 *MHz*, penukar purata kuasa dua (*RMS*) ke arus terus (*DC*), penukar analog-ke-digital 24-bit, papan litar bercetak (*PCB*) fleksibel 32 elektrod pada setiap lapisan, bekalan kuasa dan mikropengawal. Litar *EIT* digunakan untuk memperoleh pengukuran voltan menggunakan teknik pengumpulan data jiran dan bertentangan daripada tangki buatan yang terdiri daripada larutan garam (0.9% *NaCl*) dan telah diuji pada tulang *Acrylonitrile Butadiene Styrene (ABS)* cetakan 3D dan tulang kambing. Imej *EIT* buatan telah dibina semula menggunakan *pyEIT* dalam potongan tiga lapisan pada satah 3D. Kemudian, imej dianalisis prestasinya menggunakan ralat purata kuasa dua akar (*RMSE*) dan pekali korelasi. Nilai *RMSE* bagi imej yang dibina semula pada frekuensi 400 *kHz* ialah 0.2785 ± 0.01 . Daripada pekali korelasi antara tulang *ABS* dan tulang kambing, terdapat persamaan yang ketara dari segi impedans antara kedua-dua bahan dengan korelasi *Pearson* dengan nilai minimum 0.636. Adalah berfaedah untuk menggunakan bahan *ABS* untuk mensimulasikan bentuk patah tulang yang berbeza untuk dibina semula dalam sistem *EIT*. Patah boleh dilihat pada beberapa imej. Di samping itu, kedalaman tulang juga boleh dibezakan.

TABLE OF CONTENTS

	TITLE	PAGE
	DECLARATION	iii
	DEDICATION	iv
	ACKNOWLEDGEMENT	v
	ABSTRACT	vi
	ABSTRAK	vii
	TABLE OF CONTENTS	viii
	LIST OF TABLES	xi
	LIST OF FIGURES	xii
	LIST OF ABBREVIATIONS	xvi
	LIST OF SYMBOLS	xviii
	LIST OF APPENDICES	xx
CHAPTER 1	INTRODUCTION	1
	1.1 Background of the Study	1
	1.2 Problem Statement	2
	1.3 Research Objectives	3
	1.4 Scope of Study	4
	1.5 Significance of Study	4
	1.6 Thesis Outline	5
CHAPTER 2	LITERATURE REVIEW	7
	2.1 Introduction	7
	2.2 Electrical Impedance Tomography (EIT)	7
	2.2.1 Sensing Types	9
	2.3 Measurement Technique	10
	2.4 Data Acquisition Module	15
	2.4.1 Waveform Generator	16
	2.4.2 Multiplexers	17
	2.4.3 EIT Phantom Tank	18

2.5	Image Reconstruction Module	19
2.6	Reconstruction Algorithm	21
2.6.1	Finite Element Method (FEM)	21
2.6.2	Newton Raphson Method	22
2.6.3	Gauss-Newton	23
2.6.4	Graz consensus Reconstruction algorithm for EIT (GREIT)	24
2.6.5	Summary Reconstruction Algorithm	26
2.7	Medical Imaging Devices for Bone Fracture Diagnosis	26
2.8	EIT for Clinical Applications	28
2.9	Summary	34
CHAPTER 3	RESEARCH METHODOLOGY	35
3.1	Introduction	35
3.2	Research Plan and Procedure	35
3.3	Data Acquisition Module	38
3.3.1	Waveform Generator	39
3.3.2	Multiplexer Unit	41
3.3.3	Instrumentation Amplifier (IA)	44
3.3.4	Bandpass Filter	48
3.3.5	RMS to DC Converter	50
3.3.6	Analog to Digital Converter (ADC)	52
3.3.7	Power Supply	54
3.3.8	Microcontroller	56
3.4	Phantom Tank	57
3.5	Data Collection Method	59
3.6	Image Reconstruction Module	61
3.7	Performance Analysis	63
3.7.1	Root Mean Square Error (RMSE)	63
3.7.2	Correlation Coefficient between Bone and ABS	64
3.8	Summary	65

CHAPTER 4	RESULT AND DISCUSSION	67
4.1	Introduction	67
4.2	PCB Fabrication	67
4.3	Signal Data	70
4.4	Reconstructed Image	72
4.5	Analysis of RMSE	78
4.6	Correlation Coefficient between the Lamb Bone and ABS Bone Phantom	79
4.7	Limitation of Study	81
4.8	Improvement based on the Limitation of Study	85
4.9	Summary	98
CHAPTER 5	CONCLUSION AND RECOMMENDATIONS	99
5.1	Introduction	99
5.2	Conclusion	99
5.3	Future Recommendations	100
REFERENCES		103

LIST OF TABLES

TABLE NO.	TITLE	PAGE
Table 2.1	Comparison performance of the different data collection method [29].	12
Table 2.2	The technique used by several researchers.	13
Table 2.3	Comparisons of the available most used softwares and tools for image construction in EIT.	20
Table 2.4	The advantages and disadvantages of the existing imaging devices.	26
Table 4.1	The Main Differences between PCB EIT Version 1 and 2.	67
Table 4.2	The Covariance and Pearsons correlation values on each layer.	80
Table 4.3	The image reconstructed on neighboring and opposite methods using improved version of EIT tank with lamb bone on center location and full dip inside the phantom tank.	89
Table 4.4	The image reconstructed on neighboring and opposite methods using improved version of EIT tank with lamb bone on side location and full dip inside the phantom tank.	91
Table 4.5	The image reconstructed on neighboring and opposite methods using improved version of EIT tank with lamb bone on center location and half dip inside the phantom tank.	93
Table 4.6	The image reconstructed on neighboring and opposite methods using improved version of EIT tank with lamb bone on side location and half dip inside the phantom tank.	95
Table 4.7	The signal obtained from precipitated electrodes and the flex electrodes PCB electrodes.	97

LIST OF FIGURES

FIGURE NO.	TITLE	PAGE
Figure 1.1	Types of Bone Fracture [2].	2
Figure 2.1	The red dot represent the number of the electrode and the grey line indicates the connection path for four-pole and two-pole with the number electrodes 8, 16 and 32[14].	9
Figure 2.2	The neighboring/adjacent method [28].	10
Figure 2.3	The opposite/polar method [28].	11
Figure 2.4	Common ground current injection method [8].	11
Figure 2.5	EIT system basic block diagram [15].	16
Figure 2.6	Voltage current-controlled source (VCCS) block diagram [38].	16
Figure 2.7	Ag/AgCl electrode (a) Snap side (b) Skin side [49].	18
Figure 2.8	Schematic drawing of the phantom tank: Left: vertical reading, middle: circular reading in step, and Right: horizontal reading across the center [45].	19
Figure 2.9	The FEM is the most common approach to solve the partial differential equation (PDE) [56].	22
Figure 2.10	lung static image generated through Gauss-Newton [58].	24
Figure 2.11	An adult male thoraces finite element model with green rectangle represents the electrodes around the subject chest [60].	25
Figure 2.12	Comparison of images constructed between Sheffield Backprojection (SBP), Gauss-Newton (GN) and GREIT (GN) to the changes of the object radius from the center of EIT tank [60].	25
Figure 2.13	(a) Phantom agar and melon as lung (b) image reconstructed using D-bar method [70].	28
Figure 2.14	The electrical impedance computer mammograph MEIK device with 256 electrodes arranged in square matrix [72].	29
Figure 2.15	Generated adult head using finite element mesh using Absolute Undirected Hausdorff distance [75].	30
Figure 2.16	Electrical Impedance Spectroscopy (EIS) on the phantom tank and bone [77].	31

Figure 2.17	X-ray image of both phantoms: Normal femur image (left); Image of the femur with a sharp fracture (right) [77].	32
Figure 2.18	A. Five bone-electrodes placed onto rabbit femur to measure cortical bioimpedance. B. Circuit diagram with a “current source” to estimate bioimpedance modulus in vivo rabbits [78].	32
Figure 2.19	Buffalo tibial bioimpedance from intact to broken condition. From 334.1 ohm for intact, the impedance value increases to 334.7 for fractured bone [79].	33
Figure 3.1	Methodology flowchart.	36
Figure 3.2	System flow of EIT circuit to obtain the signal from EIT phantom tank.	38
Figure 3.3	Flow diagram for direct digital synthesizer (DDS).	39
Figure 3.4	Circuit schematic for direct digital synthesizer (DDS).	39
Figure 3.5	AC sinusoidal waveform generation.	40
Figure 3.6	Direct digital synthesizer (DDS) PCB.	41
Figure 3.7	Flow diagram for multiplexer unit.	42
Figure 3.8	Circuit schematic for multiplexer unit.	43
Figure 3.9	Multiplexer unit PCB.	44
Figure 3.10	Flow diagram for instrumentation amplifier a) from DDS to multiplexer and b) from demultiplexer to BPF.	45
Figure 3.11	Circuit schematic for instrumentation amplifier.	46
Figure 3.12	Instrumentation amplifier PCB.	47
Figure 3.13	Flow diagram for bandpass filter (BPF) consist of highpass filter (HPF) and lowpass filter (LPF) to filter the signal from the IA 2.	48
Figure 3.14	The lowpass and highpass filter diagram generated by Filter Pro.	49
Figure 3.15	Circuit schematic for bandpass filter (BPF).	49
Figure 3.16	PCB bandpass filter (BPF)	50
Figure 3.17	Flow diagram for RMS to DC converter to demodulate the AC signal to DC output.	51
Figure 3.18	Circuit schematic for RMS to DC converter to demodulate the AC signal to DC output.	51
Figure 3.19	RMS to DC converter PCB.	52

Figure 3.20	Flow diagram for analog-to-digital converter (ADC) using ADS1252 to provide 24-Bit resolution.	53
Figure 3.21	Circuit schematic for analog-to-digital converter (ADC) using ADS1252.	53
Figure 3.22	24-Bit ADC PCB.	54
Figure 3.23	Flow diagram for power supply to convert 5V input source to -5V, -2.5V and 2.5V to the circuit.	54
Figure 3.24	Circuit schematic for power supply.	55
Figure 3.25	Power supply PCB.	55
Figure 3.26	Arduino due and the label of pins used.	56
Figure 3.27	Dimension EIT tank consists of three layers of 16-electrodes.	57
Figure 3.28	3D printed EIT phantom tank 16 electrodes on each 3 layers (a) Asymmetric view (b) Plane view (c) Side view.	58
Figure 3.29	3D Printed EIT phantom tank connected with AgCl electrodes and the enamel wire.	58
Figure 3.30	Data collection flowchart.	60
Figure 3.31	Flowchart of the reconstruction image in pyEIT.	62
Figure 4.1	(a) Power supply, (b) Direct digital synthesis (DDS), (c) Instrumentation amplifier, (d) Bandpass filter (BPF), (e) RMS to DC converter, and (f) 24-Bit analog-to-digital converter (ADC).	69
Figure 4.2	Multiplexer circular array.	69
Figure 4.3	Full combination of the components for EIT circuit.	70
Figure 4.4	Location of the cylindrical glass bottle inside the phantom tank.	71
Figure 4.5	The impedance measurement for 16 electrodes 208 (16x13) total measurement using adjacent method.	71
Figure 4.6	The reconstruction of 2D image for glass bottle from 100 kHz to 900 kHz.	73
Figure 4.7	The reconstruction of 2D image for glass bottle from 1 MHz to 10 MHz.	74
Figure 4.8	Lamb Bone Inside the Phantom Tank.	75
Figure 4.9	Three Layers Slices of the Image Reconstruction on 3D Plane with Transparency.	76

Figure 4.10	The Slices of Image on 3D Plane for Lamb Bone and the ABS Bone using Neighboring and Opposite Methods.	77
Figure 4.11	RMSE for Glass Bottle from Frequency 100 kHz to 10 MHz.	78
Figure 4.12	The Correlation Coefficient for Layer 1 between ABS Bone and the Lamb Bone at the Same Position.	79
Figure 4.13	The Correlation Coefficient for Layer 2 between ABS Bone and the Lamb Bone at the Same Position.	79
Figure 4.14	The Correlation Coefficient for Layer 3 between ABS Bone and the Lamb Bone at the Same Position.	80
Figure 4.15	Lamb Bone with Transverse Cut Represent Transverse Fracture.	81
Figure 4.16	Lamb Bone with Crack from Neighboring and Opposite Data Collection Method.	82
Figure 4.17	Precipitation on the Electrodes Inside Phantom Tank.	83
Figure 4.18	The Electrodes Resistance Value on Layer 1.	83
Figure 4.19	The Electrodes Resistance Value on Layer 2.	84
Figure 4.20	The Electrodes Resistance Value on Layer 3.	84
Figure 4.21	Improved version of EIT tank dimension.	85
Figure 4.22	Left: The flexible PCB 32 electrodes, right: multiplexer board with FPC connector.	86
Figure 4.23	The placement of the flex electrodes on the printed EIT tank.	86
Figure 4.24	Lamb bone with transverse cut.	87
Figure 4.25	Position of the lamb bone inside the tank a) Center location with full dip, b) side location with full dip, c) Center location with half dip, and d) Side location with half dip.	87
Figure 5.1	Suggestion on the Application of EIT System on the Plaster Cast.	101

LIST OF ABBREVIATIONS

AC	-	Alternating Current
ADC	-	Analog to Digital Converter
BIA	-	Bio-Electrical Impedance Analysis
CT	-	Computerized Tomography
DBIM	-	Distorted Born Iterative Method
DDS	-	Direct Digital Synthesis
ECF	-	Extracellular Fluid
ECM	-	Extracellular Matrix
ECG	-	Electrocardiogram
EIDORS	-	Electrical Impedance and Diffuse Optical Tomography Reconstruction Software
EIT	-	Electrical Impedance Tomography
EIM	-	Electrical Impedance Mammography
EIPG	-	Electrical Impedance Plethysmography
EIS	-	Electrical Impedance Spectroscopy
EMI	-	Electromagnetic Interference
FDA	-	Food and Drug Administration
FEM	-	Finite Element Method
GREIT	-	Graz consensus Reconstruction algorithm for EIT
IA	-	Instrumentation Amplifier
ICF	-	Intracellular Fluid
ICG	-	Electrical Impedance Cardiography
ICH	-	Intercranial Hemorrhage
MIT	-	Magnetic Induction Tomography
MMG	-	Mammography
MRI	-	Magnetic Resonance Imaging
PCB	-	Printed Circuit Board
PET	-	Positron Emission Tomography
RF	-	Radio Frequency
RMSE	-	Root Mean Square Error

SR	-	Slew Rate
VCC	-	Voltage to Current Converter
VCCS	-	Using Voltage Current Controlled Source
VCO	-	Voltage-Controlled Oscillator

LIST OF SYMBOLS

I	-	Current
V	-	Voltage
Z	-	Impedance
R	-	Resistance
X_C	-	Reactant
ρ	-	Phase Angle
L	-	Length
A	-	Area
m^2	-	Meter Square
σ	-	Conductivity Distribution
ϕ	-	Electric Potential Distribution
\hat{n}	-	Current Injected
J	-	Conductivity Jacobian
$K(\sigma)$	-	Conductivity Matrix
z	-	Signal Measured
Z	-	FEM Of the Signal
W	-	Number Of Finite Elements in The Image
Q	-	Regularization Matrix
T	-	Tikhonov Style Regularization
$V_{measured}$	-	Vector of Physical Medium Voltage Measurements
σ_0	-	Original Context Conductivity Calculation
σ_r		Impedance Calculated
σ_c		Expected Impedance
$f(\sigma)$	-	Minimization of Error Function
R	-	Regularization Matrix
λ	-	Relaxation Vector Scalar
f_{max}	-	Maximum Frequency
i_c	-	Internal Capacitor
V_m	-	Maximum Peak Voltage of Signal
ΔV	-	Impedance Calculated from the Experimental Data

- ΔV^{fem} - Expected Impedance from the Reconstructed FEM Model
- cov - Covariance

LIST OF APPENDICES

APPENDIX	TITLE	PAGE
Appendix A	Arduino Data Collection Code	113
Appendix B	pyEIT Image Reconstruction Code	124
Appendix C	List of Publication	129

CHAPTER 1

INTRODUCTION

1.1 Background of the Study

Skeleton system plays important roles in human body, such as protecting the internal organs, help maintaining the body shape and is involved in body growth. But what if this system fails to operate on its normal cause by incident that led to bone fracture? The bone fractures could occur because of traumatic incidents such as sporting injuries, vehicle accidents, falls, and conditions such as osteoporosis and some types of cancer could also easily cause bone fracture [1].

Bone plays an important role in providing strong support to the soft tissues and muscles. These bones are built up from 20% of water, 80% of it are cells, lipids, and extracellular matrix (ECM) [2]. Even though the bone structures are strong, they can still break and lead to bone fracture. In the year 2019, about 1.78 million people experienced bone fracture on the forearm [3]. Moreover, 50% of children will break a bone before adulthood. In 2010, 158 million of people who exceeded 50 years of age worldwide have a high risk of osteoporotic fracture and estimated would multiple in 2040 [4]. The most common factors causing bone fracture are traumas or specific bone diseases; bone fractures could also occur because of the micro-fracture's accumulation in healthy bones, which is called 'stress fracture'. These micro-fractures commonly occur after continuous loading [2]. There are several types of bone fractures, which can be classified into several types of fractures such as transverse, stress, oblique, greenstick and comminuted [2]. Figure 1.1 illustrated the types of fractures which occur at the femur bone.

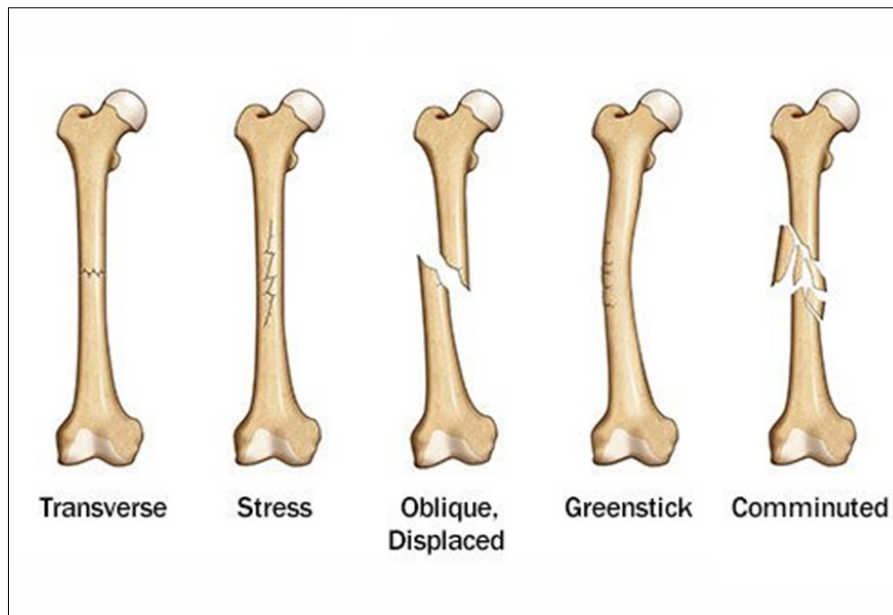


Figure 1.1 Types of Bone Fracture [2].

When bone fracture occurs, a patient will need to be diagnosed to inspect the bone's condition before and after the operation and to identify the morphology of the fracture part to determine the best treatment to be applied. There are several existing devices to perform bone imaging such as X-ray, Computerized Tomography (CT)-Scan, Positron Emission Tomography (PET)-Scan, Magnetic Resonance Imaging (MRI), Ultrasound and Electrical Impedance Tomography (EIT). In this study, will be focusing on EIT to identify the bone fracture on the upper limb.

1.2 Problem Statement

Bone healing is a natural mechanism to preserve the mechanical function of bone. This process requires cell formation and tissue remodeling [5]. Over time, this regenerative process will reform normal morphology of bone on the fracture location until the bone is completely healed. But, for the healing rate depends on bone homeostasis and several hormones in our body, which differs between each person [6]. Through the advanced imaging technology, the bone healing progress can be monitored by a physician. The common imaging devices that have been used to diagnose the bone condition such as X-rays, Computerize Tomography (CT)-Scan and Positron Emission Tomography (PET)-Scan can give good images of our internal

organs and tissues. However, overexposure of ionization radiation can lead patients to the risk of tumour, leukaemia and cancer especially to children [7]. Magnetic Resonance Imaging (MRI) is an advanced radiation-free medical device, however, is quite costly and time-consuming [8]. For monitoring the bone healing progress especially on the upper limb, it is not worth to expose the patient with radiation and high-cost device, especially for post diagnosis.

Several studies which tested EIT on bone fracture have been done, however, the number is still low and some of the studies only focus on lower limb and cranial fracture. This study aims to investigate alternative method in monitoring the condition of upper limb fracture by using EIT. To develop the circuit and the phantom model that resemble the electricity properties to the upper limb. Thus, to investigate the reconstruction images of bone fracture phantom and the most optimum range of frequency for signal measurement.

1.3 Research Objectives

The objectives of the research are:

1. To develop EIT circuit to measure the electrical impedance on the phantom model.
2. To develop phantom model of the upper limb with fractured bones using saline solution and 3D printed bones.
3. To reconstruct 2D images on each cross-section layer of the upper limb phantom using pyEIT.
4. To analyze the performance of the reconstructed model of fractured bone.

1.4 Scope of Study

This research involves the development of an upper limb phantom tank consists with saline solution and will be tested the bone fractures on the lamb bone and the ABS bone on different positions. The EIT circuit developed using Autodesk Eagle PCB consist of different compartment stack together to connect with the 16 electrodes on the EIT tank. Meanwhile, the research uses pyEIT, an open-source python package for EIT system for the image reconstruction using the Graz consensus Reconstruction algorithm for EIT (GREIT). In this research, the reconstruction only limited to the three layers, which can produce three 2D cross-sectional image on the phantom and plotted on 3D plane.

1.5 Significance of Study

This research helps to investigate an alternative method for upper limb bone condition post-diagnosis in avoiding the use of harmful radiation device to detect bone fracture. It is also used to obtain unexpensive approach in monitoring upper limb's bone fracture. It also aims to provide insights on the advantages and limitations of EIT system on bone fracture monitoring. Meanwhile, to provide enough evidence on the similarity of the reconstruction between the real bone and the ABS bone, to find an alternative method on design the phantom bone fracture for testing the reconstruction image in EIT. In addition, it aims to apply the python framework of the EIT system which is newly emerged image reconstruction tool in EIT community to test the applicability of this tool in reconstruct the EIT images.

1.6 Thesis Outline

The contents of the thesis are arranged by chapter. The contents of each chapter are as follows:

- Chapter 1 gives broad introduction of this thesis, consist of background of the study, problem statement, research objectives, scopes of study and significance of study.
- Chapter 2 presents a review on the studies related to devices used to diagnose the bone fracture. Meanwhile, discuss the fundamental and the application of the EIT such as the measurement techniques, data acquisition module, image reconstruction module and the image reconstruction algorithms.
- Chapter 3 describes the development and the experiment of the EIT system on the lamb bone and the ABS bone. This chapter discuss deeply on the circuit design, phantom design, and the reconstruction algorithms.
- Chapter 4 shows the result from the reconstructed images and discuss the outcome from the reconstruction using analytical tools. Meanwhile, address the limitation on this study.
- Chapter 5 presents the conclusion and the future recommendation to improve the limitation from this study.

REFERENCES

- [1] G. D. Chloros, A. Papadonikolakis, and G. S. Themistocleous, “Correlation of high-resolution ultrasonographic findings with the clinical symptoms and electrodiagnostic data in carpal tunnel syndrome [2],” *Ann. Plast. Surg.*, vol. 59, no. 3, pp. 351–352, 2007.
- [2] A. Oryan, S. Monazzah, and A. Bigham-Sadegh, “Bone injury and fracture healing biology,” *Biomed. Environ. Sci.*, vol. 28, no. 1, pp. 57–71, 2015.
- [3] A.-M. Wu *et al.*, “Global, regional, and national burden of bone fractures in 204 countries and territories, 1990–2019: a systematic analysis from the Global Burden of Disease Study 2019,” *Lancet Heal. Longev.*, vol. 2, no. 9, pp. e580–e592, 2021.
- [4] A. Odén, E. V Mccloskey, J. A. Kanis, N. C. Harvey, and H. Johansson, “Burden of high fracture probability worldwide : secular increases 2010 – 2040,” pp. 2243–2248, 2015.
- [5] D. D. Anderson, T. P. Thomas, A. Campos Marin, J. M. Elkins, W. D. Lack, and D. Lacroix, “Computational techniques for the assessment of fracture repair,” *Injury*, vol. 45, no. SUPPL. 2, 2014.
- [6] D. J. Kirby, D. B. Buchalter, U. Anil, and P. Leucht, “DHEA in bone: the role in osteoporosis and fracture healing,” *Int. Osteoporos. Found. Natl. Osteoporos. Found. 2020 Abstr.*, 2020.
- [7] M. Tungjai and J. Sopapang, “The Effects of Medical Diagnostic Low Dose X-rays after in vitro Exposure of Human Red Blood Cells : Hemolysis and Osmotic Fragility,” *Toxicol. Environ. Heal. Sci.*, vol. 11(3), pp. 237–243, 2019.
- [8] G. Singh, S. Anand, B. Lall, A. Srivastava, V. Singh, and H. Singh, “Practical phantom study of low cost portable EIT based cancer screening device,” *2016 IEEE Long Isl. Syst. Appl. Technol. Conf. LISAT 2016*, pp. 1–6, 2016.
- [9] R. H. Bayford, “BIOIMPEDANCE TOMOGRAPHY (ELECTRICAL IMPEDANCE TOMOGRAPHY),” *Annu. Rev. Biomed. Eng.*, vol. 8, no. 1, pp. 63–91, Jul. 2006.
- [10] S. Anand, B. Lall, A. Srivastava, and V. Singh, “A Technical Review of Various Bioelectric Impedance methods for health monitoring,” *2018 IEEE Long Isl.*

- Syst. Appl. Technol. Conf.*, pp. 1–6, 2018.
- [11] J. J. Ackmann and M. A. Seitz, “METHODS OF COMPLEX IMPEDANCE MEASUREMENTS IN BIOLOGIC TISSUE.,” *Crit. Rev. Biomed. Eng.*, vol. 11, no. 4, pp. 281–311, 1984.
- [12] E. Johnson, W. Bolonchuk, and I. Lykken, “Assessment of fat-Free mass using bioelectrical impedance measurements of the human body Assessment impedance of fat-free mass using bioelectrical measurements of the human body1 ’ 2,” no. May, 1985.
- [13] P. Davies, M. A. Preece, C. J. Hicks, and D. Halliday, “The prediction of total body water using bioelectrical impedance in children and adolescents,” *Ann. Hum. Biol.*, vol. 15, no. 3, pp. 237–240, Jan. 1988.
- [14] Y. Zhang, R. Xiao, and C. Harrison, “Advancing Hand Gesture Recognition with High Resolution Electrical Impedance Tomography,” *Proc. 29th Annu. Symp. User Interface Softw. Technol. - UIST ’16*, pp. 843–850, 2016.
- [15] M. Soleimani, “Electrical impedance tomography system: An open access circuit design,” *Biomed. Eng. Online*, vol. 5, pp. 2–9, 2006.
- [16] S. L. and D. T. Susana Aguiar Santos, Anne Robens, Anna Boehm, “System Description and First Application of an FPGA- Based Simultaneous Multi-Frequency Electrical Impedance Tomography,” *Biomass Chem Eng*, vol. 49, no. 23–6, 2015.
- [17] H. Liew Yi, “Image Reconstruction of Electrical Impedance Tomography System,” *Bachelor Thesis, Electr. Control. UTM*, no. March, 2003.
- [18] B. Lobo, C. Hermosa, A. Abella, and F. Gordo, “Electrical impedance tomography,” *Ann. Transl. Med.*, vol. 6, no. 2, pp. 26–26, 2018.
- [19] S. A. Santos *et al.*, “Monitoring Lung Contusion in a Porcine Polytrauma Model using EIT: an Application Study,” *Antonie van Leeuwenhoek, Int. J. Gen. Mol. Microbiol.*, vol. 94, no. 2, pp. 257–265, 2008.
- [20] R. F. Kushner, “Bioelectrical impedance analysis: A review of principles and applications,” *J. Am. Coll. Nutr.*, vol. 11, pp. 199–209, May 1992.
- [21] F. S. Moura, J. Cesar, C. Aya, A. T. Fleury, M. Britto, and P. Amato, “Dynamic Imaging in Electrical Impedance Tomography of the Human Chest With Online Transition Matrix Identification,” *IEEE Trans. Biomed. Eng.*, vol. 57, no. 2, pp. 422–431, 2010.
- [22] T. A. Hope and S. E. Iles, “Technology review : The use of electrical impedance

- scanning in the detection of breast cancer,” *Breast Cancer Res.*, vol. 6, no. 2, pp. 69–74, 2003.
- [23] D. Murphy and P. Physiol, “Clinical Physics and Physiological Measurement Related content Impedance imaging in the newborn,” *Clin. Phys. Physiol. Meas.*, vol. 8, pp. 131–140, 1987.
- [24] T. A. Khan and S. H. Ling, “Review on Electrical Impedance Tomography : Artificial Intelligence Methods and its Applications,” *Algorithms 2019*, vol. 12, no. 88, 2019.
- [25] M. Chien, Ñ. T. Huang, and Y. Wu, “Prevalence of Sarcopenia Estimated Using a Bioelectrical Impedance Analysis Prediction Equation in Community-Dwelling,” *JAGS*, vol. 56, no. 9, pp. 1710–1715, 2008.
- [26] U. G. Kyle *et al.*, “Bioelectrical impedance analysis F part I: review of principles and methods,” *Clin. Nutr.*, vol. 23, pp. 1226–1243, 2004.
- [27] U. G. Kyle *et al.*, “Bioelectrical impedance analysis — part II : utilization in clinical practice,” *Clin. Nutr.*, vol. 23, pp. 1430–1453, 2004.
- [28] M. Kauppinen, Hyttinen, “Impedance Tomography,” 2006. [Online]. Available: <http://www.bem.fi/book/26/26.htm>.
- [29] J. G. Webster, *Electrical Impedance Tomography*. Adam Hilger Series on Biomedical Engineering, 1990.
- [30] C. Putensen, B. Hentze, S. Muenster, and T. Muders, “Electrical impedance tomography for cardio-pulmonary monitoring,” *J. Clin. Med.*, vol. 8, no. 8, 2019.
- [31] S. J. H. Heines, U. Strauch, M. C. G. van de Poll, P. M. H. J. Roekaerts, and D. C. J. J. Bergmans, “Clinical implementation of electric impedance tomography in the treatment of ARDS: a single centre experience,” *J. Clin. Monit. Comput.*, vol. 33, no. 2, pp. 291–300, 2019.
- [32] A. Ansory, P. Prajitno, and S. K. Wijaya, “Design and development of electrical impedance tomography system with 32 electrodes and microcontroller,” *AIP Conf. Proc.*, vol. 1933, no. February, 2018.
- [33] S. P. Kumar and N. Sriraam, “Reconstruction of Brain Electrical Impedance Tomography Images Using Particle Swarm Optimization,” *2010 5th Int. Conf. Ind. Inf. Syst.*, pp. 339–342, 2010.
- [34] M. Goharian, M. Soleimani, A. Jagatheesan, K. Chin, and G. R. Moran, “A DSP Based Multi-Frequency 3D Electrical Impedance Tomography System,” *Ann.*

- Biomed. Eng.*, vol. 36, no. 9, pp. 1594–1603, 2008.
- [35] G. Ye, K. H. Lim, R. George, G. Ybarra, W. T. Joines, and Q. H. Liu, “A 3D EIT SYSTEM FOR BREAST CANCER IMAGING Gang Ye , Kim H . Lim , Rhett George , Gary Ybarra , William T . Joines and Qing H . Liu , Fellow , IEEE Department of Electrical and Computer Engineering,” *3rd IEEE Int. Symp. Biomed. Imaging Nano to Macro, 2006.*, pp. 1092–1095, 2006.
- [36] V. Chitturi and N. Farrukh, “Development of An Agilent Voltage Source for Electrical Impedance Tomography Applications,” *ARPJ. Eng. Appl. Sci.*, vol. 11, no. 5, pp. 3270–3275, 2016.
- [37] Z. Cuil, H. Wang, L. Tang, L. Zhang, X. Chen, and Y. Yan, “A Specific Data Acquisition Scheme for Electrical Tomography,” *I2MTC 2008 - IEEE Int. Instrum. Meas. Technol. Conf.*, no. c, pp. 3–6, 2008.
- [38] A. B. S. Umbu and Endarko, “The design of voltage controlled current source (VCCS) for single frequency Electrical Impedance Tomography (EIT),” *Proc. - 2017 Int. Semin. Sensor, Instrumentation, Meas. Metrol. Innov. Adv. Compet. Nation, ISSIMM 2017*, vol. 2017-Janua, pp. 30–36, 2017.
- [39] Y. Yang and J. Jia, “A multi-frequency electrical impedance tomography system for real-time 2D and 3D imaging,” *Rev. Sci. Instrum.*, vol. 88, no. 8, 2017.
- [40] A. Adler and W. R. B. Lionheart, “Uses and abuses of EIDORS: An extensible software base for EIT,” *Physiol. Meas.*, vol. 27, no. 5, 2006.
- [41] J. J. Ackmann, “Complex bioelectric impedance measurement system for the frequency range from 5 Hz to 1 MHz,” *Ann. Biomed. Eng.*, vol. 21, no. 2, pp. 135–146, 1993.
- [42] E. D. Holder, W. Lionheart, N. Polydorides, and A. Borsic, *Methods , History and Applications The Reconstruction Problem*, vol. 0750309520. Institute of Physics Publishing, 2004.
- [43] P. Studies, C. Engineering, and P. Studies, “Enhancements in Electrical Impedance Tomography (EIT) Image Reconstruction for 3D Lung Imaging,” University of Ottawa, 2007.
- [44] D. Garg and V. Goel, “Design and development of Electrical Impedance Tomography (EIT) based System,” *Int. J. Comput. Appl.*, vol. 74, no. 7, 2013.
- [45] Y. Maimaitijiang, S. Böhm, O. Jaber, and A. Adler, “A phantom based system to evaluate EIT performance,” *Physiol. Meas.*, vol. 32, pp. 851–865, 2011.

- [46] T. Yilmaz, T. Karacolak, E. Topsakal, and M. State, “Characterization of Muscle and Fat Mimicking Gels at MICS and ISM Bands (402- 2 . Tissue Mimicking Gel Characterization MICS MICS,” *Dep. ECE Mississippi State Univ.*, pp. 5–8, 2008.
- [47] T. Review, “The electric resistivity of human tissues (100 Hz- 10 MHz): a meta-analysis of review studies,” *Physiol. Meas.*, vol. 20, 1999.
- [48] H. P. Schwan, “Interface Phenomena and Dielectric Properties Of Biological Tissue,” *Encycl. Surf. Colloid Sci.*, no. 7, pp. 2643–2652, 2002.
- [49] S. Grimnes and Ø. G. Martinsen, “Electrodes,” in *Bioimpedance-and-Bioelectricity-Basics*, Elsevier, 2015, pp. 179–254.
- [50] P. Tallgren, S. Vanhatalo, K. Kaila, and J. Voipio, *Tallgren P, Vanhatalo S, Kaila K, Voipio J Evaluation of commercially available electrodes and gels for recording of slow EEG potentials. Clin Neurophysiol 116:799-806*, vol. 116. 2005.
- [51] S. Fung, A. Adler, and A. D. C. Chan, “Using Distmesh as a mesh generating tool for EIT,” *J. Phys. Conf. Ser.*, vol. 224, no. 1, 2010.
- [52] B. Liu *et al.*, “SoftwareX pyEIT : A python based framework for Electrical Impedance Tomography,” *SoftwareX*, vol. 7, pp. 304–308, 2018.
- [53] J. Rintoul, “Open EIT – Electrical Impedance Tomography,” 2020. [Online]. Available: <https://github.com/OpenEIT/OpenEIT>.
- [54] C. Dimas, P. P. Sotiriadis, and A. H. Architecture, “Electrical Impedance Tomography Image Reconstruction for Adjacent and Opposite Strategy using FEMM and EIDORS Simulation Models,” *2018 7th Int. Conf. Mod. Circuits Syst. Technol. Electr.*, pp. 2018–2021, 2018.
- [55] P.-O. Persson, “DistMesh - A Simple Mesh Generator in MATLAB,” *DistMesh - A Simple Mesh Generator in MATLAB*, 2012. [Online]. Available: <http://persson.berkeley.edu/distmesh/>.
- [56] T. de C. Martins *et al.*, “A review of electrical impedance tomography in lung applications: Theory and algorithms for absolute images,” *Annu. Rev. Control*, vol. 48, pp. 442–471, 2019.
- [57] A. Adler and R. Guardo, “Electrical impedance tomography: Regularized imaging and contrast detection,” *IEEE Trans. Med. Imaging*, vol. 15, no. 2, pp. 170–179, 1996.
- [58] P. . Darma, M. R. Baidillah, M. W. Sifuna, and M. Takei, “Real-time Dynamic

- Imaging Method for Flexible Boundary Sensor in Wearable Electrical Impedance Tomography,” *IEEE Sens. J.*, vol. 20, no. 16, pp. 9469–9478, 2020.
- [59] T. Spectroscopy, J. P. Leitzke, H. Zangl, K. Shin, and J. L. Mueller, “Related content Incorporating a priori information into the Sheffield filtered backprojection algorithm Incorporating apriori information into the Sheffield filtered backprojection algorithm,” *Physiol. Meas.*, vol. 16, pp. A111–A122, 1995.
- [60] A. Adler *et al.*, “GREIT: A unified approach to 2D linear EIT reconstruction of lung images,” *Physiol. Meas.*, vol. 30, no. 6, 2009.
- [61] C. Gómez-Leberge and A. Adler, “Direct calculation of the electrode movement Jacobian for 3D EIT,” *13th Int. Conf. Electr. Bioimpedance 8th Conf. Electr. Impedance Tomogr.*, vol. 1, pp. 364–367, 2007.
- [62] T. J. Yorkey, J. G. Webster, and W. J. Tompkins, “Comparing Reconstruction Algorithms for Electrical Impedance Tomography,” *IEEE Trans. Biomed. Eng.*, vol. BME-34, no. 11, pp. 843–852, 1987.
- [63] V. V. Raya, B. S. Iskandar, and P. D. Ridzuan, “Image Reconstruction and Resolution via Electrical Impedance Tomography,” Universiti Teknologi PETRONAS, 2012.
- [64] M. W. Vannier, “National institute of biomedical imaging and bioengineering,” *IEEE Trans. Med. Imaging*, vol. 20, no. 1, p. 1, 2001.
- [65] T. Jones and D. Townsend, “History and future technical innovation in positron emission tomography,” *J. Med. Imaging*, vol. 4, no. 1, p. 011013, 2017.
- [66] K.-H. Ng, A. C. Ahmad, M. Nizam, and B. Abdullah, “Magnetic Resonance Imaging: Health Effects and Safety,” *Proc. Int. Conf. Non-Ionizing Radiat. UNITEN*, pp. 1–15, 2003.
- [67] A. Nagiseti, “CT Scan Vs MRI Scan,” 2016. [Online]. Available: <https://www.slideshare.net/AjayNagiseti/ct-scan-vs-mri-scan>.
- [68] H. Mayo, H. Punchihewa, J. Emile, and J. Morrison, “Types of Medical Imaging,” 2018. [Online]. Available: <https://www.doc.ic.ac.uk/~jce317/types-medical-imaging.html>.
- [69] N. M. Zain, K. C. Kanaga, M. I. A. Sharifah, A. Suraya, and N. H. Latar, “Study of Electrical Impedance Tomography as a primary screening technique for breast cancer,” *2014 IEEE Conf. Biomed. Eng. Sci.*, no. December, pp. 220–224, 2014.

- [70] T. De Castro *et al.*, “Annual Reviews in Control A review of electrical impedance tomography in lung applications: Theory and algorithms for absolute images,” *Annu. Rev. Control*, vol. 48, pp. 442–471, 2019.
- [71] B. Gowry, A. B. Shahrman, and M. Paulraj, “Electrical bio-impedance as a promising prognostic alternative in detecting breast cancer: A Review,” *2015 2nd Int. Conf. Biomed. Eng.*, no. March, pp. 1–6, 2015.
- [72] N. M. Zain and K. K. Chelliah, “Breast imaging using electrical impedance tomography: Correlation of quantitative assessment with visual interpretation,” *Asian Pacific J. Cancer Prev.*, vol. 15, no. 3, pp. 1327–1331, 2014.
- [73] Y. Lit, L. Raot, R. Hetsp, and M. Get, “Image Reconstruction of EIT Using Differential Evolution Algorithm,” *Proc. 25th Annu. Int. Conf. IEEE EMBS*, pp. 1011–1014, 2003.
- [74] G. Xu, Q. Yang, Y. Li, Q. Wu, and W. Yan, “The Electrical Properties of Real Head Model Based on Electrical Impedance,” *Proc. 25th Annu. Int. Conf. IEEE EMBS*, pp. 994–997, 2003.
- [75] A. P. Gibson, J. Riley, M. Schweiger, J. C. Hebden, S. R. Arridge, and D. T. Delpy, “A method for generating patient-specific finite element meshes for head modelling,” *Phys. Med. Biol.*, vol. 48, no. 4, pp. 481–495, 2003.
- [76] D. Holder, “Clinical and Physiological Applications of Electrical Impedance Tomography,” *J. Clin. Eng.*, vol. 19, Jan. 1994.
- [77] A. H. D. Osa, A. Concu, F. R. Dobarro, and J. C. Felice, “Bone Fracture Detection By Electrical Bioimpedance: First Non-Invasive Measurements In Ex-Vivo Mammalian Femur,” *Cold Spring Harbor Lab.*, 2019.
- [78] R. A. Rinaldi and J. D. Goodrich, “Bone Electrical Conduction,” *J. Bioelectr.*, vol. 1, no. 1, pp. 83–97, Jan. 1982.
- [79] M. Khan, S. P. S. M. A. Sirdeshmukh, and K. Javed, “Evaluation of bone fracture in animal model using bio-electrical impedance analysis,” *Perspect. Sci.*, vol. 8, pp. 567–569, 2016.
- [80] D. Holder, “Electrical Impedance Tomography: Methods, History and Applications,” in *Medical Physics - MED PHYS*, vol. 32, 2005.
- [81] N. Meziane, J. G Webster, M. Attari, and A. J. Nimunkar, “Dry electrodes for electrocardiography,” *Physiol. Meas.*, vol. 34, pp. R47–R69, 2013.
- [82] M. Xiloyannis, C. Gavriel, A. A. C. Thomik, and A. A. Faisal, “Gaussian Process Autoregression for Simultaneous Proportional Multi-Modal Prosthetic

- Control with Natural Hand Kinematics,” *IEEE Trans. Neural Syst. Rehabil. Eng.*, vol. 4320, no. c, pp. 1–17, 2017.
- [83] I. Analog Devices, “Analog Devices. 2005. 32-Channel Analog Multiplexer. ADG732..,” Retrieved July 4; 2021 from https://www.analog.com/media/en/technical-documentation/data-sheets/adg726_732.pdf, pp. 1–21, 2015.
- [84] Y. Kato, T. Mukai, T. Hayakawa, and T. Shibata, “Tactile sensor without wire and sensing element in the tactile region based on EIT method,” *Proc. IEEE Sensors*, pp. 792–795, 2007.
- [85] B. Reid and M. Zhao, “The Electrical Response to Injury: Molecular Mechanisms and Wound Healing,” *Wound Heal. Soc.*, vol. 3, no. 2, pp. 184–201, 2014.
- [86] B. Panda, S. K. Dash, and S. N. Mishra, “High Slew Rate op-amp design for low power applications,” *2014 Int. Conf. Control. Instrumentation, Commun. Comput. Technol. ICCICCT 2014*, pp. 1096–1100, 2014.
- [87] C. Putensen, J. Zinserling, and H. Wrigge, “Electrical Impedance Tomography for Monitoring of Regional Ventilation in Critically Ill Patients BT - Intensive Care Medicine,” in *Intensive Care Medicine*, 2006, pp. 448–457.
- [88] S. C. Kim and T. J. Kang, “Image Analysis of Standard Pilling Photographs Using Wavelet Reconstruction,” *Text. Res. J.*, vol. 75, no. 12, pp. 801–811, 2005.
- [89] Z. Wang, A. C. Bovik, H. R. Sheikh, and E. P. Simoncelli, “Image quality assessment: From error visibility to structural similarity,” *IEEE Trans. Image Process.*, vol. 13, no. 4, pp. 600–612, 2004.
- [90] S. Ren, K. Sun, C. Tan, and F. Dong, “A Two-Stage Deep Learning Method for Robust Shape Reconstruction with Electrical Impedance Tomography,” *IEEE Trans. Instrum. Meas.*, vol. 69, no. 7, pp. 4887–4897, 2020.
- [91] O. Duongthipthewa, P. Uliss, P. Pattarasritanawong, P. Sukaimod, and T. Ouypornkochagorn, “Analysis of Current Patterns to Determine the Bladder Volume by Electrical Impedance Tomography (EIT),” *ACM Int. Conf. Proceeding Ser.*, pp. 122–127, 2020.
- [92] U. Guth, F. Gerlach, M. Decker, and W. Oelßner, “Solid-state reference electrodes for potentiometric sensors,” *J Solid State Electrochem*, vol. 13, pp. 27–39, 2009.

- [93] Y. Li *et al.*, “Analysis of measurement electrode location in bladder urine monitoring using electrical impedance,” *Biomed. Eng. Online*, vol. 18, no. 1, pp. 1–12, 2019.
- [94] H. Yeon *et al.*, “Long-term reliable physical health monitoring by sweat pore–inspired perforated electronic skins,” *Sci. Adv.*, vol. 7, no. 27, pp. 1–11, 2021.

Appendix C List of Publication

Indexed Conference Proceedings

- [1] A. H. Abdul Salam, Z. Nurul Farha, J. Mohd Najeb, A. Muhammad Amir, P. Jaysuman, and M. L. Hadafi Fitri. (2021) “16 by 3 Electrodes Electrical Impedance Tomography System Implementation on Cylindrical Phantom Design and Development,” In *2021 IEEE-EMBS Conference on Biomedical Engineering and Sciences 2020 (IECBES2020)* (pp. 3–7). IEEE. <https://doi.org/10.1109/IECBES48179.2021.9398790> (**Indexed by SCOPUS**)